Building and Environment 295 (2026) 114432

Contents lists available at ScienceDirect

Building and Environment

journal homepage: www.elsevier.com/locate/buildenv

Wind-sheltering effects of urban trees on the heating demand of building archetypes: A case study in Dublin

Zhihui Ren [a, b, *], Marialena Nikolopoulou [b], Gerald Mills [c], Francesco Pilla [a]

[a] School of Architecture, Planning and Environmental Policy, University College Dublin, Dublin, D04 V1W8, Ireland
[b] Kent School of Architecture and Planning, University of Kent, Canterbury, CT2 7NR, UK
[c] School of Geography, University College Dublin, Dublin, D04 V1W8, Ireland

HIGHLIGHTS

- Neighbourhood-scale microclimate conditions are simulated using SUEWS.
- Wind speed is associated with higher heating demand via infiltration effects.
- Tree configurations providing wind shelter are linked to lower heating demand.
- Tree characteristics influence wind sheltering and solar access.

ARTICLE INFO

Keywords:
Urban trees
Heating demand
Infiltration
Wind speed
Building energy modelling
Building archetypes

ABSTRACT

The residential sector accounts for over one-quarter of overall energy use in Ireland, making it the second-largest energy end-use behind transport. Reducing heat loss through infiltration is a critical component of building stock renovation, primarily driven by gaps in the building envelope and wind exposure. While the former can be managed through upgrades of construction, the latter can be improved through urban planning design to provide wind shelter. This study investigates the impact of urban trees on the heating energy demand of common building archetypes in Dublin, Ireland, focusing on the sheltering effects on heat loss driven by infiltration. Various tree design strategies are simulated to generate accurate weather conditions for building energy modelling. The results reveal that wind speed has a dominant influence on heat loss due to infiltration. Under windy conditions and for specific building archetypes, infiltration contributes up to 31.42% of heating demand. Within the scenarios examined, urban trees, particularly street tree configurations, are associated with reduced wind exposure and corresponding reductions in infiltration-driven heat loss of up to 6.15%. These results highlight the importance of urban evergreen trees in enhancing residential energy efficiency. This study provides valuable insights that are applicable to other urban areas with similar climatic conditions.

1. Introduction

The buildings sector, as a major global energy consumer, was responsible for over one-third of the final energy demand and 37% of total global CO_2 emissions in 2022 [1]. The increase in energy demand in buildings is driven by ongoing population growth and rapid urbanisation. Buildings are crucial in addressing climate change and supporting many Sustainable Development Goals (SDGs), owing to their substantial contributions to economic growth, social progress, and environmental protection [2]. Therefore, understanding how urban factors influence building energy demand is essential to developing optimised strategies for achieving urban sustainability goals.

Currently, heating and cooling demands constitute a significant share of societal energy consumption and are major contributors to carbon emissions under prevailing energy structures [3]. In most European countries, demand for heating significantly surpasses that for space cooling [4]. Interestingly, this trend persists even in the warmest European countries [5]. In Ireland, it is estimated that 61% of household energy use is devoted to space heating [6,7], with uncontrolled air infiltration being a key factor contributing to this high demand.

* Corresponding author at: School of Architecture, Planning and Environmental Policy, University College Dublin, Dublin, D04 V1W8, Ireland.
Email addresses: zhihui.ren@ucdconnect.ie (Z. Ren), m.nikolopoulou@kent.ac.uk (M. Nikolopoulou), gerald.mills@ucd.ie (G. Mills), francesco.pilla@ucd.ie (F. Pilla).

https://doi.org/10.1016/j.buildenv.2026.114432
Received 22 October 2025; Received in revised form 25 February 2026; Accepted 27 February 2026
Available online 28 February 2026

Infiltration, also known as air leakage, refers to air exchange through cracks or small openings in buildings. This phenomenon has been investigated through field measurement or simulation in various buildings across many cities, such as those in the UK [8], the US [9], China [10,11], and South Korea [12]. Studies consistently show that uncontrolled infiltration profoundly impacts heating and cooling loads within buildings. For instance, a study in the Mediterranean climate revealed that air infiltration could alter heating demand by 2.43 and 16.44 kWh/m^2·year and cooling demand by 0.54 and 3.06 kWh/m^2·year [13]. Jokisalo et al. reported that in typical Finnish detached houses, infiltration accounts for about 15–30% of the total energy used for space heating, including ventilation. In the UK, infiltration is responsible for 3–5% of total energy demand, 11–15% of residential energy demand, and 10–14% of housing carbon emissions [14]. It is noticed that, although the general thought is that recently built buildings have better airtightness than older ones, this is not always the case. The air permeability test of dwellings in Ireland supports this finding [15].

Infiltration is primarily driven by gaps in the building envelope and ambient wind [14,16–18]. Wind-induced pressure gradients in low-rise buildings predominantly control infiltration, outweighing stack pressure. Hadavi et al. calculated the infiltration rate using computational fluid dynamics (CFD) simulations and found a significant scale ratio of 1:2:12 for wind speeds of 1, 4, and 8 m/s across all urban layouts [19]. Miszczuk et al. conducted a parametric study on the impact of local weather conditions on energy demand in residential buildings, highlighting the significant influence of wind speed on air infiltration and heat losses [20]. In another report about simulations of residential buildings, it was shown that air leakages significantly affect the value of the peak demand for thermal power for heating purposes [21]. It is crucial to note that the strongest winds significantly increase the peak demand for thermal power due to buildings' lack of airtightness.

Given the technical and financial challenges associated with large-scale envelope retrofitting, Nature-Based Solutions (NBS) offer a cost-effective, sustainable alternative to traditional energy retrofitting methods, which is gaining increasing attention [22]. Urban vegetation can influence building energy performance through multiple mechanisms, including blocking solar radiation [23,24], providing wind sheltering effects [25,26], and altering air temperature and humidity through transpiration [27]. Currently, most research focuses on the role of vegetation in reducing cooling demand during the summer months. In contrast, the role of urban trees in modifying winter heating demand remains less well understood. Specifically, the sheltering effects may reduce the infiltration-driven heat loss, while the shading effects may simultaneously limit beneficial solar gains, potentially increasing heating demand in the winter. A year-long indoor thermal performance study conducted in Beijing, a temperate climate city, found that outdoor wind speed and solar radiation are more strongly related to indoor thermal performance in winter than outdoor air temperature [28]. Consequently, the net winter impact of vegetation reflects a trade-off between sheltering and shading effects and remains insufficiently quantified in terms of its implications for building heating demand.

Existing research on shelterbelts and windbreaks has demonstrated that reduced wind exposure can lead to substantial savings in heating energy demand. For example, a study conducted in Scotland predicted heating-season energy savings ranging from 16–42% due to the presence of shelterbelts [26]. Similarly, a study in Edinburgh reported significant reductions in heating energy demand associated with infiltration losses mitigated by shelterbelt trees, particularly in buildings with large openings [29]. However, these studies are primarily based on rural settings or isolated idealised building forms, with limited representation of the urban morphology. In addition, building energy simulations in these studies typically rely on weather-station data that do not explicitly capture microclimatic modifications induced by urban form and vegetation, thereby limiting the representation of these effects in building energy performance assessments. Consequently, in urban residential environments, the coupling between tree-induced wind sheltering, infiltration-driven heat loss, and winter heating demand at the neighbourhood scale remains insufficiently quantified.

Dublin is characterised by a mild, temperate oceanic climate with long, windy winters, which leads to sustained wind exposure during the heating season. At the same time, approximately 65% of the residential building stock was constructed before 1978 and exhibits relatively poor energy performance [30]. The combination of wind-exposed winter conditions and an ageing, energy-inefficient housing stock contributes to elevated space-heating demand and exacerbates household vulnerability to energy poverty. In 2022, the ESRI estimated that 29% of Irish households were experiencing energy poverty. Together, these climatic and building characteristics, combined with a high prevalence of energy poverty, make Dublin a representative case for assessing the potential of urban trees to mitigate wind-driven heat loss in temperate maritime cities.

Against this background, this study, which focuses on Dublin, aims to quantify the winter-time impact of urban trees on the heating energy requirements of common building archetypes, focusing on the sheltering effects on heat loss driven by infiltration. This study employs a coupled modelling framework that uses localised climate inputs derived from alternative tree layouts, and these conditions are subsequently integrated into archetype-based building energy simulations. By isolating the contribution of tree-induced wind sheltering to infiltration-related heat loss, the study provides quantitative insight into the net winter impact of evergreen trees on building heating demand. The resulting evidence base supports microclimate-sensitive, nature-based measures that complement conventional retrofitting, especially for older, poorly insulated housing stock and households at risk of fuel poverty, and is transferable to cities with similar climates, informing policies for energy sustainability and climate resilience.

The remainder of this paper is organised as follows: Section 2 details the methodology, including the research roadmap, ENVI-met simulations and building energy simulations. Section 3 presents the results and discussion, focusing on the scenario simulation outcomes of both microclimate and building energy consumption, as well as the impact of trees on heating demand under various weather conditions. Section 4 concludes the key findings, outlines limitations, and offers future work.

2. Methodology

2.1. Research roadmap

This study proposed a co-simulation framework for analysing the multi-scale interactions between urban microclimate and building energy performance, specifically focusing on the sheltering effects of vegetation on the building energy demand of Irish houses in winter. Different vegetation configurations are explored to assess their impact on microclimate and heating energy demand. Fig. 1 shows the detailed steps for the framework, showing how the co-simulation process progresses from weather data preparation to final building energy analysis.

Step 1: Preparing the model input data.

In this step, several weather scenarios representing typical Irish winter conditions are considered: cold, cold and windy, and windy (Details shown in Fig. 4). These scenarios are selected to reflect the variability in Irish winter weather, particularly focusing on the combined effects of wind and cold on building energy demand. High-resolution climate projections for Ireland indicate a potential increase in the frequency of winter extra-tropical cyclones producing compound wind and rainfall extremes, which could lead to stronger future winds [31,32]. Given this projection, we selected weather data from 2020, which was the windiest year in the past two decades, as a representative basis for the windy scenarios. The geometric layouts of buildings, extracted from GIS shapefiles, provide the input data for subsequent simulations.

Step 2: Creating neighbourhood microclimate data.

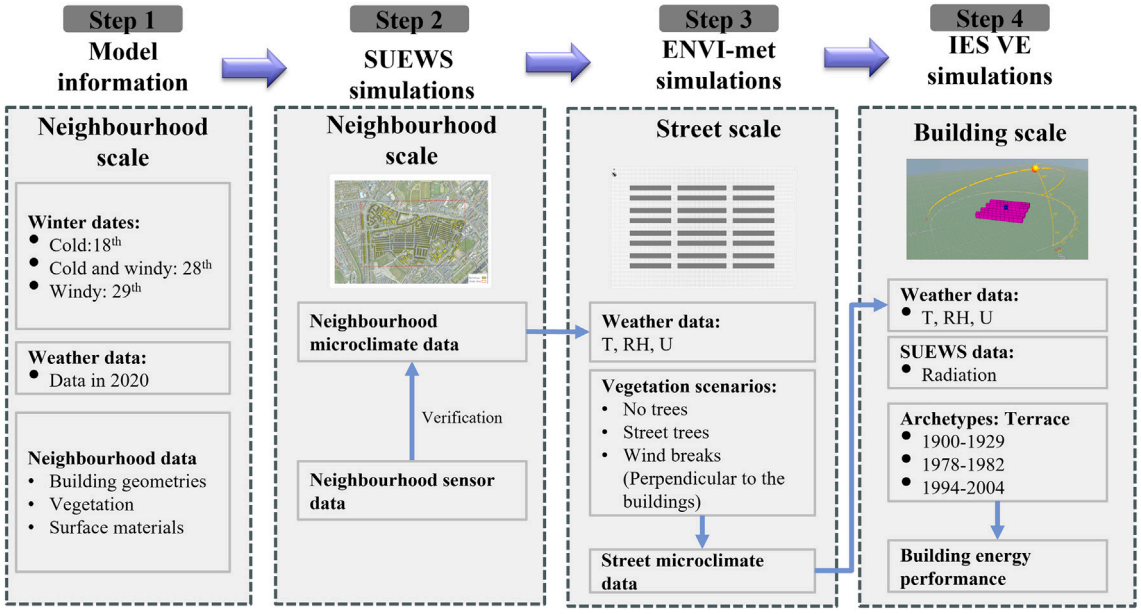

Fig. 1. The research Roadmap.

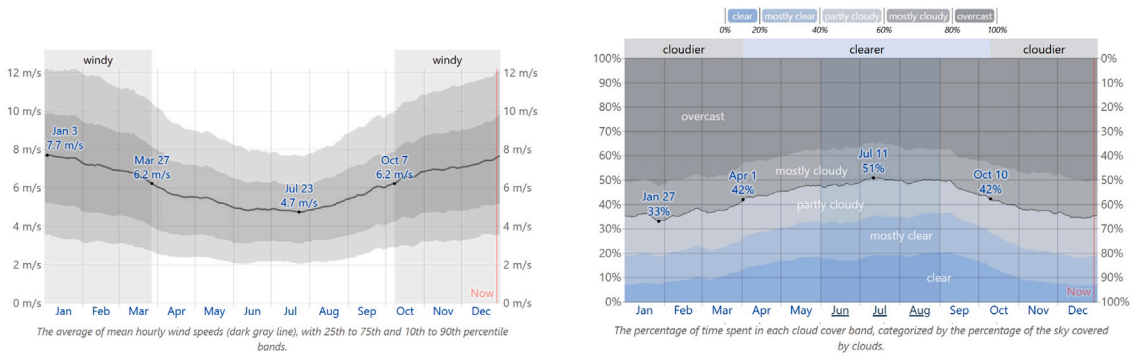

(a) (b)

Fig. 2. The wind speed (a) and cloud cover (b) in Dublin in 2020.

Using the model information in Step 1, Surface Urban Energy and Water Balance Scheme (SUEWS) simulations at the neighbourhood scale are conducted to create the local microclimate, including temperature, relative humidity, and wind conditions. The microclimate data serve as the boundary conditions for the next step. Additionally, sensor data from the study area is collected to validate and calibrate the simulation results, ensuring that the microclimate generated accurately reflects real-world conditions.

Step 3: Estimating the effects of vegetation on microclimate

The weather data generated in Step 2 is used in ENVI-met simulations at the street scale to assess the effects of various vegetation configurations, such as street trees and windbreaks, on the microclimate around buildings. These configurations are modelled to examine how vegetation influences temperature regulation, wind speed reduction, and shading. The microclimate data generated here is then used as input for the building energy simulations in Step 4.

Step 4: Estimating the effects of vegetation on heating demand

The data obtained in Step 3 is fed into the Integrated Environmental Solutions Virtual Environment (IES VE) software to simulate the heating energy demand of different building archetypes. Scenarios are developed using the building stock database of Ireland and the TABULA building archetypes to model a range of typical residential buildings. This step involves a comprehensive analysis of the heating energy demand, considering various vegetation configurations and their impact on energy savings.

2.2. Study area

Ireland (northwestern Europe) has a mild but changeable maritime climate (*Cfb*), characterised by mild summers, cool winters, and a long-term mean annual air temperature of approximately 9.7 °C. Due to the unique geographical location, Ireland experiences frequent extra-tropical cyclones during the cold season [33]. The sustained winds and extensive cloud cover constrain winter solar gains [34]. Dublin (53.35° N, 6.26° W) is located on the east coast of Ireland. The windier part of the year lasts for almost 6 months in Dublin, spanning from October to March, with average wind speeds of more than 6.2 m/s (Fig. 2(a)). During this period, Dublin also experiences a higher percentage of cloud cover, about 60% or more (Fig. 2(a)). In Ireland, approximately one-third of the residential building stock predates 1970 and suffers from subpar insulation performance [35]. With high population density and a large share of older housing, Dublin is particularly

(a) Neighbourhood context (Stoneybatter) (b) Representative street view used in scenario design.

Fig. 3. Study area imagery from Google Earth (accessed: *1 July 2025)*.

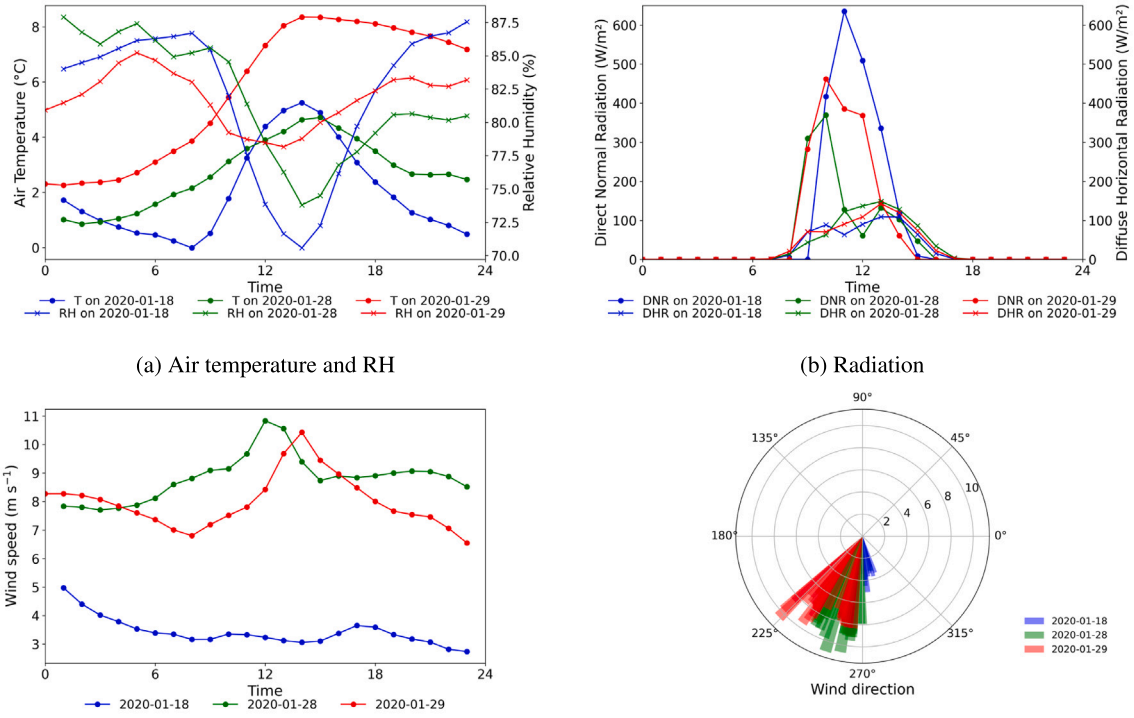

(a) Air temperature and RH (b) Radiation

(c) Wind speed (d) Wind direction

Fig. 4. Hourly air temperature and relative humidity (a), radiation (b), wind speed (c), and wind direction (d) for the simulation days.

affected. These stock characteristics, combined with weather conditions, exacerbate the heating demand in the city.

The study neighbourhood is Stoneybatter, on the north side of Dublin city centre (as shown in Fig. 3). The area is dominated by pre-1970 terraced housing and exhibits relatively poor building energy performance [36]. These characteristics make Stoneybatter a pertinent testbed for evaluating microclimate-sensitive interventions aimed at reducing wind-driven infiltration losses and heating demand. Details of the building stock typology are provided in Section 2.4.1.

2.3. ENVI-met simulations

2.3.1. Model description

The microclimate simulation model used in this study is ENVI-met 5.6.1. Based on the hydromechanics and thermodynamic equations, ENVI-met simulates the "surface-vegetation-atmosphere" interaction with a high temporal and spatial resolution (up to 0.5 m). ENVI-met is widely recognised in urban microclimate research due to its detailed modelling capabilities, including evapotranspiration, sensible heat fluxes, transpiration, and soil-plant water exchange [37–39]. One of the main advantages of ENVI-met is its ability to model vegetation in detail, which is essential for accurately simulating the cooling effects of vegetation on urban microclimates. Toparlar et al. [40] reviewed CFD analyses that confirm that ENVI-met is the software most used for studying the urban microclimate.

Given the high requirement of computational resources for CFD models, this study selects specific days to represent typical weather conditions in Dublin. To evaluate the impacts of low temperatures and high wind on heating demand, the selected days correspond to periods with low temperatures (referring to 18th and 28th Jan) and with high values of wind speed (referring to 28th and 29th Jan), as shown in Fig. 4.

2.3.2. Simulation verification

Usually, the majority of building energy modelling relies on typical meteorological year (TMY) data derived from nearby weather stations, which primarily represent regional background conditions and do not explicitly reflect the influence of urban morphology and land-cover characteristics on local climate. In this study, the SUEWS model is employed to generate neighbourhood-scale microclimate conditions by translating urban surface properties into local meteorological forcing, including air temperature, humidity, wind conditions, and surface radiation components. The performance and applicability of the SUEWS model for the study area have been evaluated in a previous study by Ren et al. [36]. Therefore, SUEWS is used here as a validated tool to provide representative local boundary conditions for subsequent ENVI-met and building energy simulations.

To validate the feasibility of ENVI-met, we simulated a 150 m × 150 m area centred around the weather sensor. The observation date is 26 December 2023. Environmental sensor data were obtained from a personal weather station hosted on the Weather Underground platform, which provides real-time measurements of air temperature, relative humidity, wind speed, and wind direction [41]. The data were collected from the Weather Underground weather station (ID: IDUBLI9; 53.372° N, 6.313° W), located within the study area. The air temperature, relative humidity, wind speed, and direction generated from the SUEWS are used as the input meteorological data for the ENVI-met validation model. The model runs for 24 hours, and the results for the last 18 hours are compared with the observed data collected from the neighbourhood sensor.

As the Fig. 5 shows, there is a strong correlation between the data from the simulation and the sensor. The R^2 values for the air temperature and relative humidity are both appropriately 0.82, indicating a good fit between the model and the observed data. The Mean Bias Error (MBE) of air temperature is approximately 1.1 °C, which indicates that the predicted air temperature closely matches the actual values, although with a slight overestimation. This overestimation may be due to the influence of various factors in the actual urban environment, such as human activities and local wind conditions. It is also important to note that the sensor data naturally exhibits fluctuations. In addition, the ENVI-met model does not account for all environmental variables and human interferences during simulations, such as traffic conditions. Despite these limitations, the simulations performed using ENVI-met are considered reliable for assessing the microclimate.

2.3.3. Design of the study cases

ENVI-met software is used to establish the initial model of the typical street scale (as shown in Fig. 3) in the neighbourhood. Based on the preliminary simulations, the grid size is set to 3 m × 3 m × 2 m, with a simulation area of 192 m×290 m. The buildings are represented as 2-floor terraces, reflecting the existing building archetypes (further details in Section 2.3.1. The building orientations are set to northeast-southwest (NE-SW) and northwest-southeast (NW-SE), aligning with the current building orientations in the neighbourhood.

Note: BD: Building Direction; TP: Tree Planting.

Currently, most trees in the neighbourhood are deciduous trees, which do not provide sheltering effects during the winter months. The existing vegetation in Stoneybatter primarily consists of street trees and park trees, serving as windbreaks. To estimate the sheltering effects of trees in winter and their impact on heating demand, this study investigates several evergreen tree planting scenarios. Table 1 shows the details of the cases. It should be noted that the sheltering effects of street trees depend on their spatial relationship with surrounding buildings. The configuration presented here should therefore be interpreted as an illustrative example, and alternative tree–building arrangements may produce different energy outcomes.

- **Case A and Case D** represent the current situation, with no vegetation.
- **Case B and Case E** introduce street trees.
- **Case C and Case F** implement windbreaks that are oriented perpendicular to the prevailing wind.

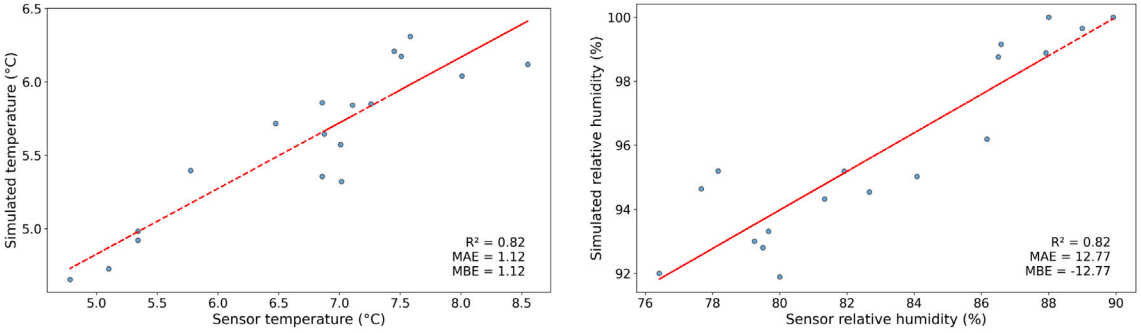

(a) T from simulation and sensor (b) RH from simulation and sensor

Fig. 5. The validation of air temperature (a) and RH (b).

Table 1
The evergreen tree planting scenarios.

Cases	Case A	Case B	Case C	Case D	Case E	Case F
BD	NE-SW	NE-SW	NE-SW	SE-NW	SE-NW	SE-NW
TP	No trees	Street trees	Windbreak	No trees	Street trees	Windbreak
Figs.	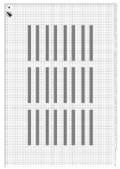	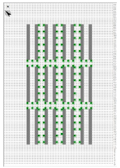	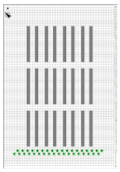	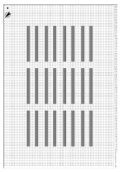	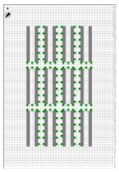	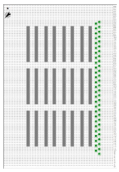

Table 2
Initial conditions used in ENVI-met.

Category	Parameter Name	Data
Basic Parameters	Location	Dublin, Ireland
	Grid size	3 m x 3 m x 2 m
	Start simulation date	18th, 28th and 29th
	Start simulation time	18:00:00
	Total simulation time	30 hours
	Model rotation	45° and 135°
Output Timing	Receptors and buildings	Every 30 min
	All other files	Every 60 min

The choice of vegetation species for the simulations is based on the site situation(road width), planting characteristics centring on Dublin and the characteristics of software grid settings. For street tree cases, we use the Cypress (height: 7 m, width: 3 m), and for windbreak cases, we use the Pine (height: 15 m, width: 7 m). To maintain consistency across all cases and avoid discrepancies due to variations in plant shape, the same plant model from the Albero tool is used for all vegetation types. All other vegetation parameters, including leaf area index (LAI), drag resistance and porosity, are adopted from the default values provided in the Albero database. It should be noted that, as the analysis focuses on winter conditions and evergreen tree species, seasonal variations in vegetation properties are outside the scope of this study. The resulting wind-sheltering effects are therefore interpreted in a relative, scenario-based manner.

To minimise edge effects and ensure the validity of the simulations, 8 nested grids were added in the calculation domain. All simulations were conducted using the standard ENVI-met atmospheric boundary layer formulation and identical numerical solver settings, time-step configuration, and convergence criteria as defined by the system defaults, ensuring numerical consistency and reproducibility across all cases. The parameters near the surface of the middle building in the terraces are extracted, including air temperature, relative humidity, and wind speed. These meteorological data are then used as input for the building energy simulations. The primary initial conditions for the simulations are summarised in Table 2, with the remaining conditions set to the default values of the system.

2.4. Building energy simulation

In this study, the Integrated Environmental Solutions Virtual Environment (IES VE) version 2023.5.2.0 was chosen to explore the sheltering effects of trees on building energy consumption of archetypes [42]. IES VE offers comprehensive analysis capabilities, including detailed evaluation and optimisation of building energy efficiency, comfort, ventilation, and HVAC performance [43,44]. It has been widely used and recommended for its high accuracy in energy modelling [42,45].

This research employs a coupling approach between ENVI-met and IES VE, where key weather variables—such as air temperature, relative humidity, and wind speed—generated by ENVI-met serve as input data for building energy simulations in IES VE. This coupling enables a more accurate representation of how outdoor microclimates, influenced by trees, impact indoor energy consumption. Specifically, it allows for precise quantification of how changes in the urban microclimate affect energy demand, particularly during colder periods when heating demand is most significant.

2.4.1. Building typology

Buckley et al. [46] present a geographic building database for Dublin city centre using a typology approach. Fig. 6 shows the distribution of buildings in Stoneybatter. This area contains 2090 buildings, of which 94% are single-family houses, with the remaining buildings being non-residential structures and apartment blocks. Terraced houses are the most common archetypes, accounting for 93.3% of the total, which aligns with the common building typology in Dublin.

Approximately 80.8% of the buildings were constructed before 1978, when building regulations were not yet in place. As a result, these older buildings typically have poor energy performance. For instance, 52.3% of the terraced houses were built before 1930, with solid brick walls (some without insulation) and single-glazed windows. In contrast, 9.0% of the terraced houses were built between 1994 and 2004, featuring cavity walls and improved energy performance due to the first Building Regulations introduced in 1992, which addressed fuel conservation and energy efficiency in buildings. The multi-family apartment blocks in the area account for just 1.2% of the total and were built after 1978, incorporating modern updates such as cavity walls and double-glazed windows. Table 3 provides the breakdown of buildings per archetype across different construction periods.

For this study, we focus on three representative archetypes of terraced houses: those built between 1900-1929, 1978-1982, and 1994–2004. These houses dominate, and the periods represent significant changes in building practices and regulations, making them particularly relevant for further analysis. Additional details on building parameters are provided in the next section.

2.4.2. Model settingup

To ensure an effective coupling between ENVI-met and the IES VE model, the building models within IES VE were configured to align with

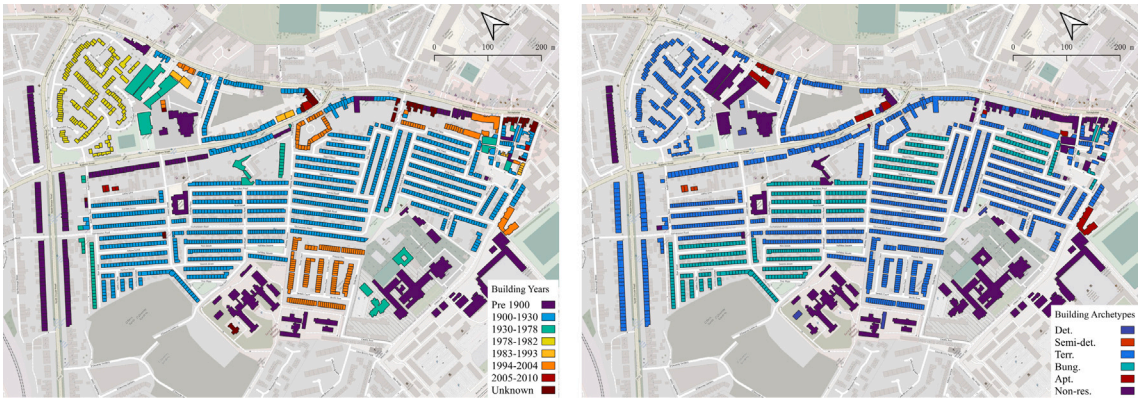

(a) The map of building years (b) The map of building archetypes

Fig. 6. The map of building years (a) and building archetypes (b). Det., Semi-det., Terr., Bung., Apt., and Non-res. denote detached, semi-detached, terraced, bungalow, apartment, and non-residential buildings, respectively.

Table 3
Number of buildings per building archetype across different years.

Years	Detached	Semi-detached	Terraced	Bungalow	Apartment	Non-Res
Pre 1900	5	–	134	–	–	51
1900–1929	–	–	960	481	–	–
1930–1978	–	–	17	22	1	18
1978–1982	–	–	149	–	–	1
1983–1993	–	8	–	–	4	–
1994–2004	–	–	188	–	10	2
2005–2010	1	–	–	–	11	–
Unknown	–	–	–	–	–	27

those in ENVI-met, as illustrated in Fig. 7. To account for the impact of surrounding buildings on energy performance, a 50 m area surrounding the target building was selected for the building energy simulation. Figs. 7(c) and Fig. 7(d) show the location of the target building within the model.

Solar radiation:

Trees influence solar radiation by blocking incoming short-wave radiation and modifying the radiative environment around buildings, thereby affecting building energy consumption. To incorporate the impact of trees on radiation, the tree positions in the IES VE model were matched to those in the ENVI-met model, as shown in Fig. 7(b) and Fig. 7(d). In the IES VE model, trees are represented as external shading elements to account for the effects on solar radiation, while microclimatic processes related to trees are calculated through ENVI-met simulation.

Infiltration:

As building standards become more stringent, the role of infiltration in building energy consumption is becoming increasingly significant. Typically, an infiltration target or standard is defined in models, represented by a mean air change rate with a 'continuously on' profile. In this study, we enhance the model resolution by implementing a dynamic infiltration profile, which is adjusted based on wind pressure derived from the model's weather file.

$$P = C \cdot \frac{1}{2}\rho v^2 \tag{1}$$

where P is wind pressure (Pa), ρ is air density (kg/m^3), v is wind speed (m/s)

ATTMA [47] utilises the power law equation to establish the relationship between the airflow Q and building pressure differentials ΔP, as given by:

$$Q = C\Delta p^n \tag{2}$$

where Q is airflow rate (m^3/s), C is flow coefficient, ΔP is the indoor–outdoor pressure difference across the building envelope (Pa), n is pressure exponent, typically ranging from 0.5 to 1. For most buildings, n is typically around 0.65 [48].

Eqs. (1) and (2) are used to calculate the wind pressure and airflow at both average and maximum wind speeds. We employ a Python script to scale the infiltration based on wind speed, as described in Eq. (3).

$$ws\_ach = \text{max\_ach} \times \left(\frac{ws\_pressure}{\text{max\_wind\_pressure}}\right)^{0.65} \tag{3}$$

where, ws_ach is wind-speed-adjusted air changes per hour, max_ach is maximum air changes per hour, $ws\_pressure$ is wind pressure at the current wind speed, and max_wind_pressure is maximum wind pressure.

Based on the analysis in Section 3.2.2, this study selects the three most common building archetypes for further investigation. All parameter values (shown in Table 4) are derived from the Building Regulations [49–52], the TABULA project [53], and other relevant studies [15,54]. In addition, air infiltration rates are determined using the Kronvall and Persily (K–P) "divide-by-20" rule of thumb [55,56], which typically uses q_{50} as the numerator [57]. These values define the baseline (mean) infiltration level for each archetype, which is subsequently modulated using Eq. (3) to generate a wind-speed-dependent infiltration profile. The resulting profile can be imported into IES VE as a freeform infiltration profile, replacing the default 'continuously on' profile. This approach allows for a more dynamic and realistic simulation of infiltration rates, improving model resolution and accuracy. Detailed occupant behaviour data for the archetypes are as outlined in Table 5.

3. Results and discussion

3.1. Results of microclimate

This section shows the results of microclimate simulations under six different cases of tree design. Air temperature and wind speed values were extracted from ENVI-met receptor grids located within one grid

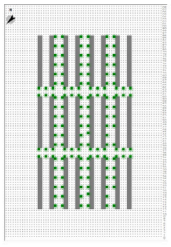

(a) ENVI-met model in 2D

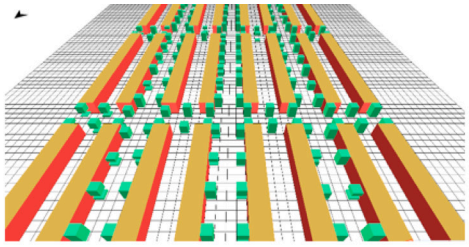

(b) ENVI-met model in 3D

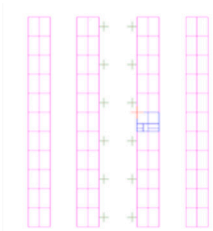

(c) IES VE model in 2D

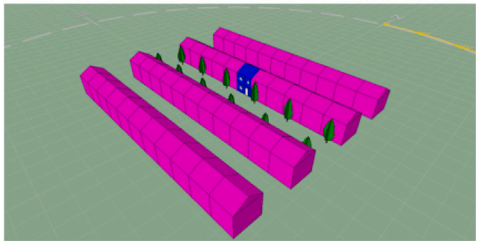

(d) IES VE model in 3D

Fig. 7. The coupled models in ENVI-met and IES VE. (The building in blue is the objective building, while the buildings in pink are the Adjacent buildings.).

Table 4
The description for the building archetypes.

Archetype	Year	Description	U-values ($W/m^2 \cdot K$)					WWR (%)	Air Permeability
			Wall	Roofs	Ground Floors	Windows	Doors		($m^3/h \cdot m^2$)
1	1900–1929	Terraced House	2.1	0.68	1.38	4.8	3	11.8	15
2	1978–1982	Terraced House	1.1	0.4	0.86	3.7	3	31.3	12
3	1994–2004	Terraced House	0.55	0.26	0.66	2.8	3	20.9	10

Table 5
The occupant behaviour data.

Description	Details	Occupant schedules
Heating point	19°C	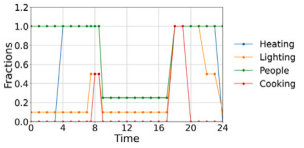
Internal heat gain	People: Max sensible heat gain 90 W/person, Max latent heat gain 60 W/person, Occupancy 4 persons Lighting: 10 W/m^2 Cooking: 10 W/m^2	

cell adjacent to the building façades and spatially averaged across all façades.

3.1.1. Air temperature

Fig. 8(a) shows the air temperature of Cases A - F on the 18th, 28th, and 29th of January. A comparison between building orientations (Cases A, B, C versus D, E, F) indicates that orientation-related differences in air temperature are small. Across the selected days, the maximum difference between Case A and Case D remains below 0.2 °C, with a peak difference of approximately 0.16 °C observed on 18 January. While the building orientation generally affects shading, it appears to have a minimal impact on air temperature in this context. This suggests that within the simulated winter conditions, building orientation plays a secondary role compared to other factors such as wind flow and tree placement.

The presence of evergreen trees, however, has a noticeable effect on air temperature. Due to the combined effects of shading, sheltering, and transpiration of trees, the air temperature around buildings varies. Fig. 8(b) shows the air temperature differences between cases with trees (Cases B, C, E, and F) and those without trees (Cases A and D). During the night, the cases with trees generally exhibit slightly warmer temperatures compared to those without. For example, on the 18th, the temperature differences reached approximately 0.05 °C for Case B and 0.03 °C for Case E during nighttime. This is likely due to reduced longwave radiation loss and stored heat in tree canopies.

During daytime hours (09:00–18:00), both street-tree configurations (Cases B and E) and windbreak configurations (Cases C and F) are associated with modest reductions in air temperature relative to the

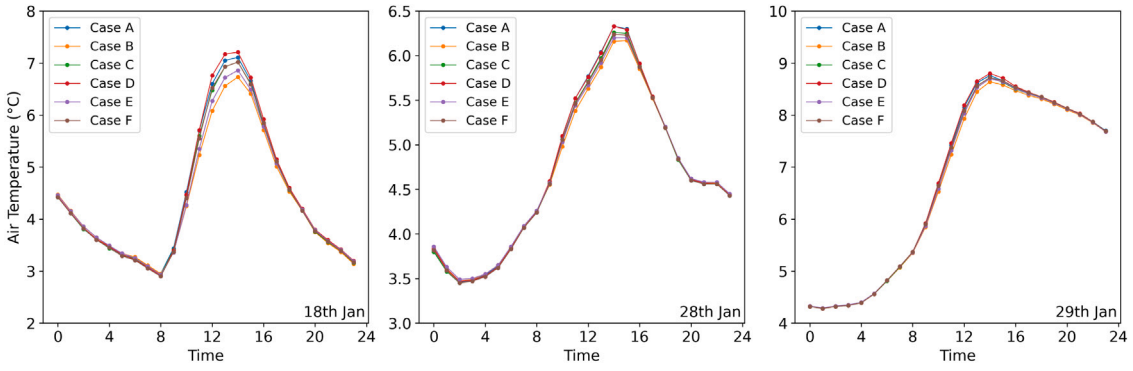

(a) Hourly air temperature for Cases A-–F on 18, 28 and 29 January.

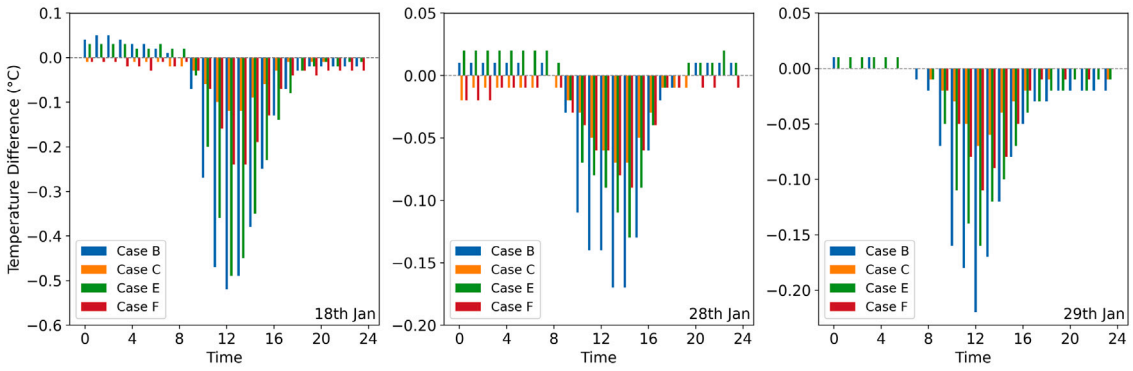

(b) Hourly air temperature differences between tree cases (B, C, E, F) and no-tree reference cases (A, D) on 18, 28 and 29 January 2020.

Fig. 8. Hourly air temperature (a) and temperature differences (b) across six building–tree configuration scenarios on selected winter days.

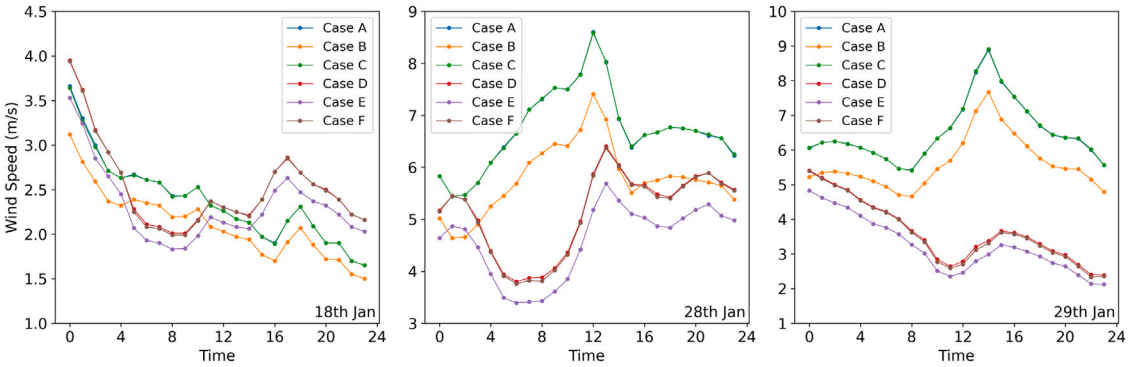

(a) Hourly wind speed for Cases A-–F on 18, 28 and 29 January.

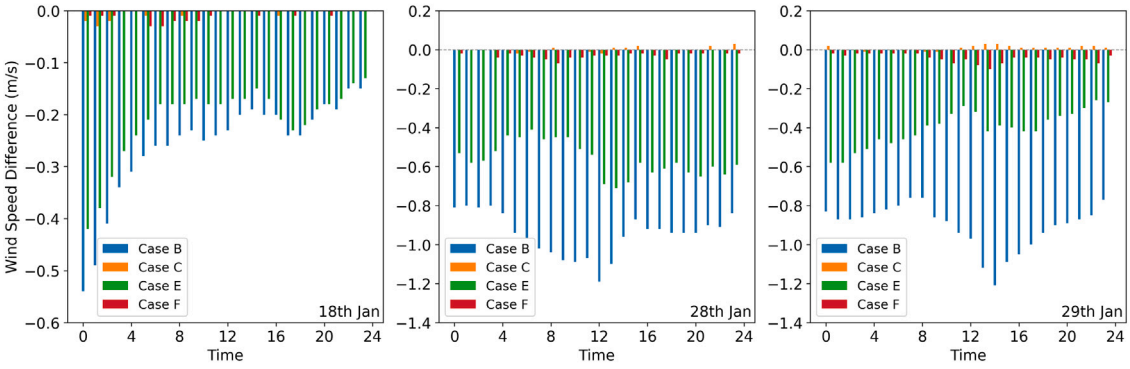

(b) Hourly wind speed differences between tree cases (B, C, E, F) and no-tree reference cases (A, D) on 18, 28 and 29 January 2020.

Fig. 9. Hourly wind speed (a) and wind speed differences (b) across six building–tree configuration scenarios on selected winter days.

baseline cases. The largest differences occur around midday, with temperature reductions ranging from approximately 0.1 °C to 0.5 °C across the analysed days. Compared to windbreak scenarios, street-tree cases exhibit more uniform temperature reductions over the daytime period, although the overall magnitude of cooling remains limited within the investigated configurations.

The temperature reductions are more pronounced on the 18th of Jan, when wind speeds are low, with temperature differences reaching 0.5°C at midday. In contrast, during windier conditions, as observed on the 28th and 29th of Jan, the temperature reductions are less noticeable, with temperature differences generally between −0.1°C and −0.2°C during midday. The wind tends to disperse the cooling effect, reducing its overall impact. These findings suggest that external climatic factors, such as solar radiation, ambient temperature, and wind speed, impact the role of tree effects on shaping air temperature.

3.1.2. Wind speed

Fig. 9(a) shows the hourly wind speed variations for Cases A - F on the 18th, 28th, and 29th of January. The overall wind speed varies across the three days. Wind conditions vary substantially across the three days, reflecting differences in background meteorological forcing. On 18 January, wind speeds remain relatively low throughout the day, with mean values of approximately 2 m/s and limited variation between cases.

In contrast, on the 28th and 29th, when wind speeds are higher, clearer differences emerge between cases with varying building orientations. Cases A, B, and C, which have a NE-SW building orientation, generally experience higher wind speeds, likely due to less interference between NE-SW-oriented buildings and the southwest wind flow. Wind speeds are consistently lower in cases with a southeast-northwest (SE-NW) orientation, suggesting that the building layout in this orientation plays a significant role in blocking wind flow.

During the same day, Case A and Case D exhibit higher wind speeds throughout the day, indicating that the absence of trees allows wind to flow with minimal obstruction. Fig. 9(b) shows the wind speed differences between cases with trees and those without trees (Case A and Case D). Cases B and E demonstrate the largest reductions in wind speed, especially during peak wind periods. The presence of street trees effectively blocks the wind flow, leading to a reduction of up to 0.5 m/s on the 18th and even greater reductions (approaching 1.2 m/s) on the 28th and 29th of January. In comparison, Case C and Case F show a slight reduction in wind speed, indicating that the windbreak plays a role in moderating wind flow, though not as significantly as street trees. It should be noted that the windbreak's effectiveness is influenced by the distance between the trees and the building.

Generally, Case B exhibits larger wind speed reductions than Case E, which can be attributed to the building orientation. The wind interacts more directly with the trees in the NE-SW building orientation, amplifying the obstruction effect. For Case F, the buildings in SE-NW orientation play an important role in reducing wind speed, with the windbreak further enhancing this effect. It is also noteworthy that there are instances of positive wind speed differences in Case C at certain hours. When buildings are oriented in the NE-SW orientation, the windbreak to the wind direction might create gaps or channels where the wind is funnelled [58]. These funnelling effects become more pronounced under higher wind conditions.

3.2. Results of building energy consumption

3.2.1. Heating loads comparison

This section compares the building energy consumption, specifically focusing on heating demand, under different tree planting scenarios

using the coupled ENVI-met and IES VE models. This study specifically examines the energy performance of the most common architectural archetypes: terraced houses built between 1900—1929, 1978—1982, and 1994—2004. Old buildings are often less energy-efficient due to their age and construction style. The analysis focuses on comparative heating-demand differences between scenarios, reflecting relative responses to changes in wind exposure under the simulated conditions.

Fig. 10 presents the daily heating load for three building archetypes (Archetype 1, 2, and 3) across six cases (A–F) on 18th January, 28th January, and 29th January. Archetype 1 exhibits the highest daily heating load across all cases and days, reaching over 60 kWh on the 28th of January. This is likely due to higher infiltration rates or less efficient insulation. In contrast, Archetype 2 shows moderate heating loads, nearly half that of Archetype 1, owing to updates in building construction. Archetype 3 demonstrates the lowest heating loads, typically below 20 kWh, suggesting better insulation or a more efficient design.

When comparing the two groups of building orientations, those with NE-SW orientations generally have higher heating loads than those with SE-NW orientations, particularly during windier conditions. The building layout plays an important role in sheltering, which reduces wind exposure and infiltration.

Although buildings with the SE-NW orientation tend to have lower heating loads overall, the group cases with the NE-SW orientation generally show a significant reduction in heating load when trees are present. This is because the buildings in the SE-NW orientation play a sheltering effect as well, thus diminishing the role of trees. While both Case B and Case E have street trees, the heating load reduction rate for Case E is almost half that of Case B.

Trees impact the air temperature and wind speed around buildings, which in turn affects heating demand. Fig. 11 shows the heating load difference rate between cases with trees and those without trees (Case A and Case D). Across the analysed days and archetypes, cases with street trees are associated with lower heating loads relative to the corresponding baseline cases, particularly for Case B compared to Case A, with a maximum reduction of 6.15% observed on 28 January. This reduction is consistent with reduced wind exposure under the simulated conditions and its influence on wind-driven heat loss. These results illustrate the potential sensitivity of heating demand to vegetation-induced changes in local wind conditions within the modelled scenarios.

However, not all tree cases contribute to reduced heating loads. For example, Case C shows a slight increase in heating load (less than 0.1 kWh) across all days compared to Case A, despite including a windbreak. This pattern suggests that stronger wind conditions are associated with increased infiltration-related heat loss under the analysed winter scenarios. Another exception is observed for Cases B and E of Archetype 3 on the 18th of January. Due to its higher energy performance, Archetype 3 experiences less heat loss driven by infiltration. In contrast, the reduction in air temperature and solar gain due to the presence of street trees leads to a higher heating demand.

In addition, all archetypes show various results under different tree cases. Taking the 28th as an example, when the weather was cold and windy, Archetype 1 experiences a 4.29% reduction in heating load due to the addition of street trees, while Archetype 3, which has better airtightness, shows a 5.99% reduction due to having lower heating loads to begin with.

3.2.2. Infiltration comparison

Infiltration contributes to building heating demand, particularly under cold and windy conditions. Fig. 12 illustrates the distribution of hourly heating loss by infiltration of all archetypes on the 18th, 28th and 29th of January. Due to the poor airtightness, Archetype 1 consistently exhibits the highest hourly infiltration across all cases and days, making it the most susceptible to infiltration losses. Archetype 2 shows a moderate infiltration level, while Archetype 3, with better insulation or resistance to air infiltration, has the lowest infiltration. For example, the median hourly infiltration of the current situation for Archetype 1 on the 28th of January is 0.8 kW, compared to approximately 0.6 kW for Archetype 3. Additionally, Archetype 1 shows the largest spread (interquartile range), while Archetype 3 demonstrates more consistent infiltration regardless of external conditions or tree placements.

Infiltration is strongly influenced by wind speed. Case B with street trees exhibits significantly lower infiltration compared to Case A without

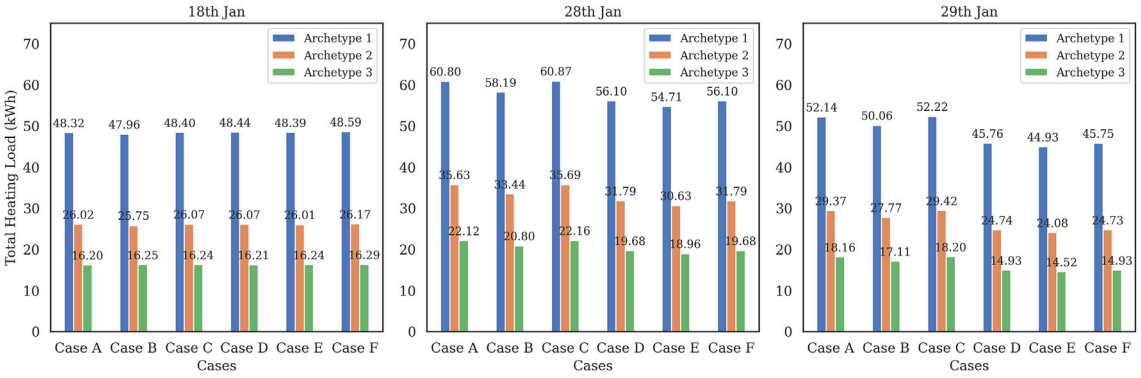

Fig. 10. Daily cumulative room heating load for three representative terraced house archetypes under six tree configuration cases on the 18th, 28th, and 29th of January.

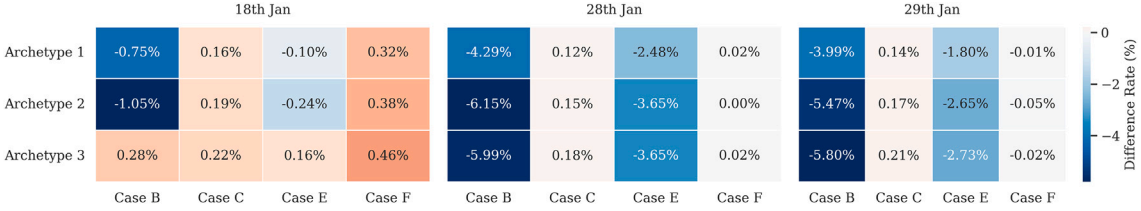

Fig. 11. Heating load difference rate for cases with trees (B, C, E, F) relative to their corresponding no-tree cases (A for B and C; D for E and F) on 18, 28, and 29 January. The difference rate is calculated as the percentage change in daily total room heating load with respect to the corresponding no-tree case.

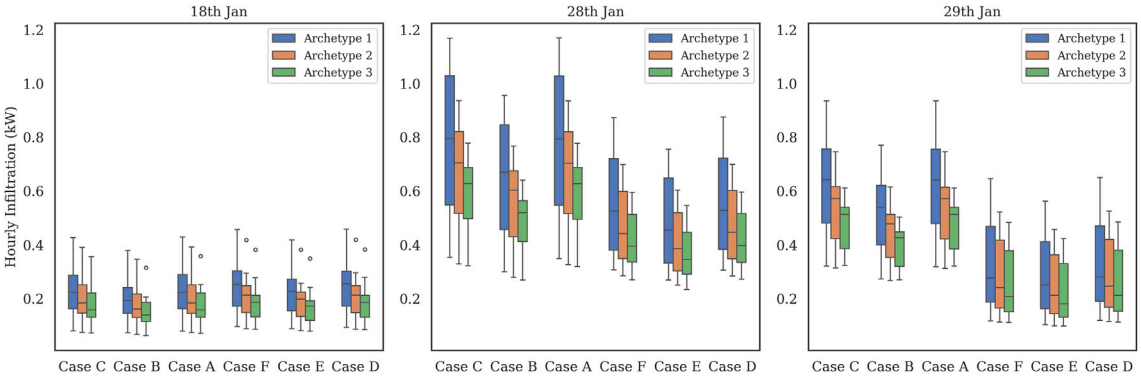

Fig. 12. The distribution of hourly infiltration heat loss for a representative terraced house archetype under six tree configuration cases on the 18th, 28th, and 29th of January. Boxplots show the distribution of hourly values across all simulated hours, with the interquartile range (box) and median (horizontal line).

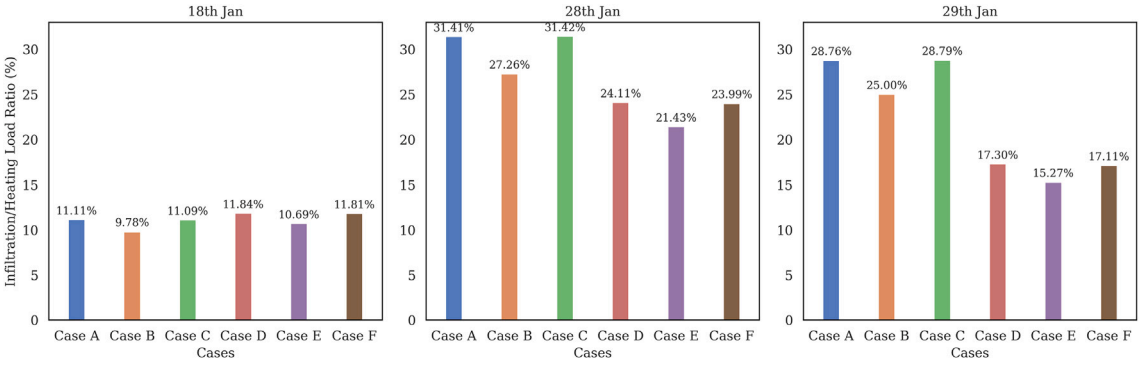

Fig. 13. Daily cumulative ratio of infiltration heat loss to room heating load for the representative Archetype 1 building on 18, 28, and 29 January.

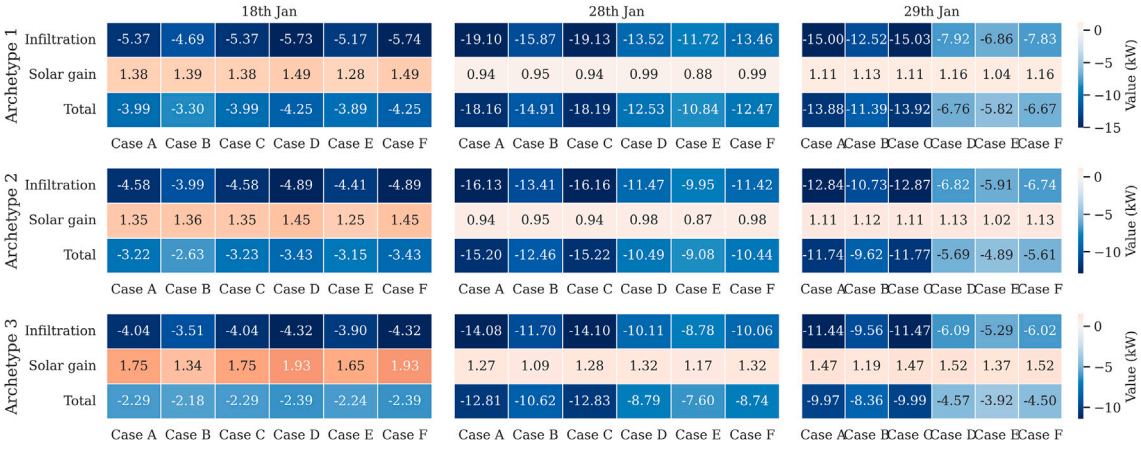

Fig. 14. Daily infiltration heat loss and solar gains of the three building archetypes on 18, 28, and 29 January.

trees. Trees effectively shelter buildings from wind, thereby reducing the heat loss driven by infiltration. Buildings with SE-NW orientation (Cases D, E, F) are more resistant to infiltration compared to those with NE-SW orientation (Cases A, B, C), highlighting the role of building alignment in mitigating wind-driven infiltration.

Usually, the uncontrolled infiltration significantly affects the heating load in buildings. Fig. 13 shows the ratio of infiltration to room heating load for the terraced house built in 1900 and 1929 (Archetype 1). On the 28th, the infiltration accounts for 21.43% to 31.42% of the heating load, which is primarily driven by gaps in the building envelope and ambient wind. The presence of street trees leads to a significant reduction in this ratio across all dates, highlighting the sheltering effects of trees in mitigating infiltration-driven heat loss.

Generally, vegetation plays the co-function of shading effects and wind-sheltering effects in winter, especially the evergreen trees. To explore the vegetation's impact on building heating demand in winter, both infiltration and solar gains under all cases are examined, as shown in Fig. 14. It is obvious that the cases with street trees have a reduction in infiltration of all archetypes, varying across the dates. Windbreaks, due to their distance from the buildings, have a less pronounced effect.

While trees reduce infiltration, they also block and absorb solar radiation, which reduces solar gains, potentially increasing heating demand during winter. For example, on the 18th of January, solar gain in Case D (the current situation) is 1.49 kWh, while it is reduced to 1.28 kWh in the case with street trees. The effect of trees on solar gain is not uniform across all environments, which varies depending on building orientation. For Archetype 1, Case B (NE-SW orientation) has a solar gain of 1.39 kWh, while Case E (SE-NW orientation) has 1.28 kWh on the 18th. This difference is due to the greater exposure to solar radiation in the NE-SW orientation compared to the SE-NW orientation.

The building archetypes impact the solar gains as well, especially the window-to-wall ratio (WWR), which directly impacts the access of solar gains to the rooms. For instance, Archetype 3, with a higher WWR, experiences more solar radiation, resulting in a solar gain of 1.75 kWh on the 18th of January, compared to 1.38 kWh and 1.35 kWh for Archetypes 1 and 2, respectively.

3.3. Impact of trees on heating demand under various weather conditions

It is well established that weather conditions play a determining role in building energy demand. Temperature fluctuations, wind speed, and solar radiation all interact with the building's physical properties and landscape design, such as tree placements, to influence the overall building energy performance. Understanding these weather-related influences is essential for optimising building energy consumption and improving climate-resilient designs.

Air temperature may be a direct factor impacting heating demand. Colder external temperatures increase the heating load required to maintain indoor comfort. On the 18th of January, with the lowest temperatures, the heating demand for all cases was nearly identical. The effects of trees on heating demand are minimal on this day, indicating that temperature was the dominant factor influencing heating needs.

Wind speed is a major factor determining the heat loss from buildings. As wind speeds increase, the heat loss due to infiltration also rises, particularly in poorly insulated buildings. The findings show that the higher wind speeds on the 28th and 29th lead to a higher infiltration, especially for Archetype 1, over 19 kWh, as shown in Fig. 14. Conversely, street trees significantly reduce wind-driven heat loss, providing a sheltering effect that lowers heating demand.

In addition, Fig. 10 shows that the 28th and 29th have a higher heating load than the 18th of Jan, despite the latter having the lowest daily air temperature. The ratio of infiltration to heating load was highest on the 28th, at about 31.4%, as seen in Fig. 13, compared to 9.8% to 11.8% on the 18th—less than half of that on the 28th. This pattern suggests that stronger wind conditions are associated with increased infiltration-related heat loss under the analysed winter scenarios. Simson et al. [21] found that the impact of high wind speeds and low sheltering conditions leads to up to 50% of all heat losses, aligning with the findings of this study.

Solar radiation can help reduce heating demand during winter by offering free passive solar heat. However, the presence of trees can block solar radiation to some degree, which may reduce the available heat. Due to a higher cloudy cover rate in Dublin during winter, the shading effects of trees are not as significant. This effect is more pronounced in buildings with SE-NW orientation, where shading from trees limits solar radiation during midday.

The combined effects of air temperature, wind speed, and solar radiation create complex interactions that influence heating demand. For example, on 28 January, when temperatures were low and wind speeds were high, heating loads reached their peak, particularly for Archetype 1. In contrast, trees provided a mitigating effect by reducing wind-driven heat loss, although this benefit was partially offset by reduced solar radiation. These findings illustrate the trade-off between wind sheltering and solar gain under the analysed winter conditions, indicating that both effects should be considered when interpreting vegetation impacts on heating demand in urban environments.

These results are particularly significant for cities like Dublin, where much of the housing stock predates modern energy efficiency standards and building retrofit options are often constrained by cost. Within this context, vegetation-induced reductions in wind-driven heat loss may represent a complementary pathway to influence heating demand, particularly for older and more permeable buildings. While not a substitute for building-level retrofitting, such microclimate-based interventions highlight the potential for landscape strategies to contribute to reducing heating energy demand and associated costs under winter conditions.

4. Conclusion

This study investigates the impact of urban trees on the heating energy demand of common building archetypes, focusing on the sheltering effects on heat loss driven by infiltration. Employing the ENVI-met model, we simulate various tree design strategies, considering the building orientation and tree placement, to generate accurate weather conditions around buildings for energy modelling. The localised climate data obtained from these simulations are then used to perform energy simulations for building archetypes in Ireland, providing a comprehensive evaluation of the role of urban evergreen vegetation in influencing heating energy demand.

This study indicates that the primary mechanism through which urban trees influence winter heating demand is wind sheltering. The presence of trees decreases near-building wind speed, which in turn mitigates heat loss driven by air infiltration. Within the simulated scenarios examined, street tree configurations were associated with the largest relative reductions in heating demand, with reductions of up to 6.16%. Heating demand is fundamentally driven by external air temperature, with colder external temperatures leading to increased heating loads, while wind speed further amplifies heating demand by increasing infiltration-related heat loss, especially in poorly insulated buildings. Under windy conditions, infiltration accounted for up to 31.42% of the heating demand in the most wind-exposed cases, underscoring its critical role in shaping winter energy requirements. While trees reduce wind-driven heat loss, their shading effect may also limit beneficial solar radiation entering buildings in winter, partially offsetting energy savings. In the present case, characterised by frequent winter cloud cover in Dublin, the shading effect of evergreen trees had a limited influence on heating demand. Overall, the effectiveness of urban tree configurations in reducing winter heating demand is closely linked to local wind exposure within the climatic context examined.

However, it is important to acknowledge the limitations of this study. Firstly, the simplification of the models is one of the non-negligible factors. This study does not explicitly resolve variations in canopy structure or fine-scale aerodynamic interactions within the tree crown, which may influence the magnitude of wind-sheltering effects. Secondly, this study focuses on the winter period using evergreen tree species, and therefore does not address potential seasonal variations in vegetation properties or their influence on wind sheltering across different times of the year. Thirdly, the assumptions regarding thermal bridge and air infiltration can lead to differences between simulations and the real values. Additionally, the influence of street trees and windbreak distance and spatial configuration relative to buildings was not systematically explored, despite its known importance for the effectiveness of wind sheltering in reducing infiltration-driven heat loss.

In future research, we aim to explore more comprehensive scenarios by integrating various factors, including a sensitivity analysis of tree characteristics and urban neighbourhood configurations, to identify the optimal urban tree design strategies. In addition, urban building energy modelling will be essential for evaluating the effectiveness of tree design and enhancing our understanding of the interactions between urban vegetation, local microclimate, and building energy consumption.

While this study focuses on Dublin, the findings may be applicable to other urban areas with similar climatic conditions. The methodology used here is particularly suited for designing pathways to reduce

energy demand across Europe, as the Tabula Tool provides building archetypes for 21 European countries. These insights are especially relevant for vulnerable populations who cannot afford the high costs of deep retrofitting. Microclimate-sensitive urban planning measures, such as strategic tree planting, may complement conventional retrofitting strategies by addressing wind-driven heat loss in vulnerable housing contexts.

CRediT authorship contribution statement

Zhihui Ren: Writing – review & editing, Writing – original draft, Visualization, Validation, Software, Methodology, Formal analysis, Data curation, Conceptualization. **Marialena Nikolopoulou:** Writing – review & editing, Supervision, Conceptualization. **Gerald Mills:** Writing – review & editing, Supervision, Methodology, Data curation, Conceptualization. **Francesco Pilla:** Writing – review & editing, Writing – original draft, Supervision, Methodology, Data curation, Conceptualization.

Declaration of competing interest

The authors declare that they have no known competing financial interests or personal relationships that could have appeared to influence the work reported in this paper.

Acknowledgements

This work was supported by the China Scholarship Council (No.: 202006120038).

Data availability

Data will be made available on request.

References

[1] United Nations, 2019 Global Status Report for Buildings and Construction Sector, Technical Report, 2019, https://www.unep.org/resources/publication/2019-global-status-report-buildings-and-construction-sector.

[2] F. Scrucca, C. Ingrao, G. Barberio, A. Matarazzo, G. Lagioia, On the role of sustainable buildings in achieving the 2030 UN sustainable development goals, Environ. Impact Assess. Rev. 100 (2023) 107069, https://doi.org/10.1016/j.eiar.2023.107069, https://www.sciencedirect.com/science/article/pii/S0195925523000355.

[3] J. Xiong, S. Guo, Y. Wu, D. Yan, C. Xiao, X. Lu, Predicting the response of heating and cooling demands of residential buildings with various thermal performances in China to climate change, Energy 269 (2023) 126789, https://doi.org/10.1016/j.energy.2023.126789, https://www.sciencedirect.com/science/article/pii/S0360544223001834.

[4] T. Abergel, A. Brown, P. Cazzola, S. Dockweiler, J. Dulac, A. Fernandez Pales, M. Gorner, R. Malischek, E.R. Masanet, S. McCulloch, L. Munera, U. Remme, R. Schuitmaker, T. Stanley, J. Teter, K. West, Energy Technology Perspectives 2017: Catalysing Energy Technology Transformations, OECD, 2017.

[5] C. Prades-Gil, J.D. Viana-Fons, X. Masip, A. Cazorla-Marín, T. Gómez-Navarro, An agile heating and cooling energy demand model for residential buildings. Case study in a Mediterranean city residential sector, Renew. Sustain. Energy Rev. 175 (2023) 113166, https://doi.org/10.1016/j.rser.2023.113166, https://www.sciencedirect.com/science/article/pii/S1364032123000229.

[6] Sustainable Energy Authority of Ireland, Ireland's Energy Statistics, Technical Report, 2022, https://www.seai.ie/data-and-insights/seai-statistics/.

[7] X. Cao, X. Dai, J. Liu, Building energy-consumption status worldwide and the state-of-the-art technologies for zero-energy buildings during the past decade, Energy and Buildings 128 (2016) 198–213, https://doi.org/10.1016/j.enbuild.2016.06.089, https://www.sciencedirect.com/science/article/pii/S0378778816305783.

[8] W. Pan, Relationships between air-tightness and its influencing factors of post-2006 new-build dwellings in the UK, Build. Environ. 45 (2010) 2387–2399, https://doi.org/10.1016/j.buildenv.2010.04.011, https://www.sciencedirect.com/science/article/pii/S0360132310001186.

[9] W.R. Chan, J. Joh, M.H. Sherman, Analysis of AIR leakage measurements of US houses, Energy and Buildings 66 (2013) 616–625, https://doi.org/10.1016/j.enbuild.2013.07.047, https://www.sciencedirect.com/science/article/pii/S0378778813004386.

[10] S. Shi, C. Chen, B. Zhao, AIR infiltration rate distributions of residences in Beijing, Build. Environ. 92 (2015) 528–537, https://doi.org/10.1016/j.buildenv.2015.05.027, https://www.sciencedirect.com/science/article/pii/S0360132315300068.

[11] H.K. Dai, C. Chen, AIR infiltration rates in residential units of a public housing estate in hong kong, Build. Environ. 219 (2022) 109211, https://doi.org/10.1016/j.buildenv.2022.109211, https://www.sciencedirect.com/science/article/pii/S0360132322004474.

[12] G. Hong, B.S. Kim, Field measurements of infiltration rate in high rise residential buildings using the constant concentration method, Build. Environ. 97 (2016) 48–54, https://doi.org/10.1016/j.buildenv.2015.11.027, https://www.sciencedirect.com/science/article/pii/S036013231530189X.

[13] J. Feijó-Muñoz, C. Pardal, V. Echarri, J. Fernández-Agüera, R. Assiego de Larriva, M. Montesdeoca Calderín, I. Poza-Casado, M.Á. Padilla-Marcos, A. Meiss, Energy impact of the AIR infiltration in residential buildings in the Mediterranean area of Spain and the canary islands, Energy Build. 188-189 (2019) 226–238, https://doi.org/10.1016/j.enbuild.2019.02.023, https://www.sciencedirect.com/science/article/pii/S0378778818337599.

[14] B. Jones, P. Das, Z. Chalabi, M. Davies, I. Hamilton, R. Lowe, A. Mavrogianni, D. Robinson, J. Taylor, Assessing uncertainty in housing stock infiltration rates and associated heat loss: English and UK case studies, Build. Environ. 92 (2015) 644–656, https://doi.org/10.1016/j.buildenv.2015.05.033, https://www.sciencedirect.com/science/article/pii/S0360132315002541.

[15] D. Sinnott, M. Dyer, Air-tightness field data for dwellings in Ireland, Build. Environ. 51 (2012) 269–275, https://doi.org/10.1016/j.buildenv.2011.11.016, https://www.sciencedirect.com/science/article/pii/S0360132311004008.

[16] K. Hassouneh, A. Alshboul, A. Al-Salaymeh, Influence of infiltration on the energy losses in residential buildings in Amman, Sustain. Cities Soc. 5 (2012) 2–7, https://doi.org/10.1016/j.scs.2012.09.004, https://www.sciencedirect.com/science/article/pii/S2210670712000601.

[17] E. Cuce, Role of airtightness in energy loss from windows: experimental results from in-situ tests, Energy Build. 139 (2017) 449–455, https://doi.org/10.1016/j.enbuild.2017.01.027, https://www.sciencedirect.com/science/article/pii/S0378778816309215.

[18] S. Khoshdel Nikkho, M. Heidarinejad, J. Liu, J. Srebric, Quantifying the impact of urban wind sheltering on the building energy consumption, Appl. Therm. Eng. 116 (2017) 850–865, https://doi.org/10.1016/j.applthermaleng.2017.01.044, https://www.sciencedirect.com/science/article/pii/S1359431117302843.

[19] M. Hadavi, H. Pasdarshahri, Quantifying impacts of wind speed and urban neighborhood layout on the infiltration rate of residential buildings, Sustain. Cities Soc. 53 (2020) 101887, https://doi.org/10.1016/j.scs.2019.101887, https://www.sciencedirect.com/science/article/pii/S2210670719316294.

[20] A. Miszczuk, D. Heim, Parametric study of AIR infiltration in residential buildings—the effect of local conditions on energy demand, Energies 14 (2021) 127, https://doi.org/10.3390/en14010127, https://www.mdpi.com/1996-1073/14/1/127. number: 1.

[21] R. Simson, T. Rebane, M. Kiil, M. Thalfeldt, J. Kurnitski, The impact of infiltration on heating systems dimensioning in Estonian climate, E3S Web of Conferences 172 (2020) 05004, https://doi.org/10.1051/e3sconf/202017205004, https://www.e3s-conferences.org/articles/e3sconf/abs/2020/32/e3sconf_nsb2020_05004/e3sconf_nsb2020_05004.html.

[22] Q. He, F. Tapia, A. Reith, Quantifying the influence of nature-based solutions on building cooling and heating energy demand: a climate specific review, Renew. Sustain. Energy Rev. 186 (2023) 113660, https://doi.org/10.1016/j.rser.2023.113660, https://www.sciencedirect.com/science/article/pii/S1364032123005178.

[23] H. Akbari, S. Konopacki, Calculating energy-saving potentials of heat-island reduction strategies, Energy Policy 33 (2005) 721–756, https://doi.org/10.1016/j.enpol.2003.10.001, https://www.sciencedirect.com/science/article/pii/S0301421503003033.

[24] T. Ichinose, L. Lei, Y. Lin, Impacts of shading effect from nearby buildings on heating and cooling energy consumption in hot summer and cold winter zone of China, Energy Build. 136 (2017) 199–210, https://doi.org/10.1016/j.enbuild.2016.11.064, https://www.sciencedirect.com/science/article/pii/S037877881631711X.

[25] D.R. DeWalle, G.M. Heisler, Windbreak effects on AIR infiltration and space heating in a mobile home, Energy Build. 5 (1983) 279–288, https://doi.org/10.1016/0378-7788(83)90015-4, https://www.sciencedirect.com/science/article/pii/0378778883900154.

[26] F. Wang, Modelling sheltering effects of trees on reducing space heating in office buildings in a windy city, Energy and Buildings 38 (2006) 1443–1454, https://doi.org/10.1016/j.enbuild.2006.03.028, https://www.sciencedirect.com/science/article/pii/S0378778806000995.

[27] A. Aboelata, S. Sodoudi, Evaluating urban vegetation scenarios to mitigate urban heat island and reduce buildings' energy in dense built-up areas in Cairo, Build. Environ. 166 (2019) 106407, https://doi.org/10.1016/j.buildenv.2019.106407, https://www.sciencedirect.com/science/article/pii/S0360132319306171.

[28] W. Li, Z. Zhou, C. Wang, Y. Han, Impact of outdoor microclimate on the performance of high-rise multi-family dwellings in cold areas and optimization of building passive design, Build. Environ. 248 (2024) 111038, https://doi.org/10.1016/j.buildenv.2023.111038, https://www.sciencedirect.com/science/article/pii/S036013232301065X.

[29] Y. Liu, D.J. Harris, Effects of shelterbelt trees on reducing heating-energy consumption of office buildings in scotland, Appl. Energy 85 (2008) 115–127, https://doi.org/10.1016/j.apenergy.2007.06.008, https://www.sciencedirect.com/science/article/pii/S0306261907000931.

[30] N.P. Buckley, Modelling Dublin: A Workflow for the Application of an Urban Building Energy Model to Evaluate Carbon Mitigation Strategies at Neighbourhood Scales. (Ph.D. thesis). University College Dublin, 2021.

[31] C. Manning, E.J. Kendon, H.J. Fowler, J.L. Catto, S.C. Chan, P.G. Sansom, Compound wind and rainfall extremes: drivers and future changes over the UK and Ireland, Weather Clim. Extremes 44 (2024) 100673, https://doi.org/10.1016/j.wace.2024.100673, https://www.sciencedirect.com/science/article/pii/S2212094724000343.

[32] P. Nolan, P. Lynch, C. Sweeney, Simulating the future wind energy resource of Ireland using the COSMO-CLM model, Wind Energy 17 (2014) 19–37, https://doi.org/10.1002/we.1554. eprint: https://onlinelibrary.wiley.com/doi/abs/10.1002/we.1554. https://onlinelibrary.wiley.com/doi/pdf/10.1002/we.1554.

[33] Met Éireann, Climate of Ireland. Available at: https://www.met.ie/climate/climate-of-ireland (Accessed 4 March 2026).

[34] P.E. Bett, H.E. Thornton, The climatological relationships between wind and solar energy supply in britain, Renew. Energy 87 (2016) 96–110, https://doi.org/10.1016/j.renene.2015.10.006, https://www.sciencedirect.com/science/article/pii/S0960148115303591.

[35] Central Statistics Office, Housing stock census of population 2022, 2023, https://www.cso.ie/en/releasesandpublications/ep/p-cpp2/censusofpopulation2022profile2-housinginireland/housingstock/.

[36] Z. Ren, M. Nikolopoulou, G. Mills, F. Pilla, Evaluating the influence of urban trees and microclimate on residential energy consumption in Dublin neighbourhoods, Build. Environ. 269 (2025) 112441, https://doi.org/10.1016/j.buildenv.2024.112441, https://www.sciencedirect.com/science/article/pii/S0360132324012824.

[37] L. Pastore, R. Corrao, P.K. Heiselberg, The effects of vegetation on indoor thermal comfort: the application of a multi-scale simulation methodology on a residential neighborhood renovation case study, Energy Build. 146 (2017) 1–11, https://doi.org/10.1016/j.enbuild.2017.04.022, https://www.sciencedirect.com/science/article/pii/S0378778817312550.

[38] J. Ge, Y. Wang, H. Akbari, D. Zhou, Z. Gu, X. Meng, Cooling energy saving by vegetation planting in high-density districts: evaluation using the coupled simulation, Build. Environ. 232 (2023) 110054, https://doi.org/10.1016/j.buildenv.2023.110054, https://www.sciencedirect.com/science/article/pii/S0360132323000811.

[39] J. Ge, Y. Wang, D. Zhou, Z. Gu, X. Meng, Effects of urban vegetation on microclimate and building energy demand in winter: an evaluation using coupled simulations, Sustain. Cities Soc. 102 (2024) 105199, https://doi.org/10.1016/j.scs.2024.105199, https://www.sciencedirect.com/science/article/pii/S2210670724000295.

[40] Y. Toparlar, B. Blocken, B. Maiheu, G.J.F. van Heijst, A review on the CFD analysis of urban microclimate, Renew. Sustain. Energy Rev. 80 (2017) 1613–1640, https://doi.org/10.1016/j.rser.2017.05.248, https://www.sciencedirect.com/science/article/pii/S1364032117308924.

[41] Weather Underground, Personal Weather Station (PWS) Network. Available at: https://www.wunderground.com/pws/overview (Accessed 24 February 2026).

[42] Integrated Environmental Solutions (IES), IES Virtual Environment (VE), version 2023.5.2.0, 2023. Available at: https://www.iesve.com/ (Accessed 24 February 2026).

[43] A. Al-Janabi, M. Kavgic, A. Mohammadzadeh, A. Azzouz, Comparison of EnergyPlus and IES to model a complex university building using three scenarios: free-floating, ideal AIR load system, and detailed, J. Build. Eng. 22 (2019) 262–280, https://doi.org/10.1016/j.jobe.2018.12.022, https://www.sciencedirect.com/science/article/pii/S2352710218311112. tLDR: This study provides new information regarding capabilities of two extensively used BPS tools to model advanced and innovative buildings, and in particular HVAC systems that are increasingly becoming used in high-performance commercial and institutional buildings worldwide.

[44] Y. Schwartz, R. Raslan, Variations in results of building energy simulation tools, and their impact on BREEAM and LEED ratings: a case study, Energy and Buildings 62 (2013) 350–359, https://doi.org/10.1016/j.enbuild.2013.03.022, https://www.sciencedirect.com/science/article/pii/S0378778813001904.

[45] S. Alavirad, S. Mohammadi, P.-J. Hoes, L. Xu, J.L.M. Hensen, Future-proof energy-retrofit strategy for an existing Dutch neighbourhood, Energy Build. 260 (2022) 111914, https://doi.org/10.1016/j.enbuild.2022.111914, https://www.sciencedirect.com/science/article/pii/S0378778822000858.

[46] N. Buckley, G. Mills, R. Fealy, An inventory of buildings in Dublin city for energy management, Irish Geography 53 (2020) 5–22, https://irishgeography.ie/index.php/irishgeography/article/view/1408., doi:http://nbn-resolving.de/urn:irg:ie:0000-igj.v53i1.14085. number: 1.

[47] ATTMA, Measuring AIR permeability of building envelopes: technical standard 1, 2016, https://www.labc.co.uk/sites/default/files/ATTMA.technical-standard-L1-permeability-envelopes-dwellings-v1-041016.pdf.

[48] M. Orme, M. Liddament, A. Wilson, TN 44: numerical data for AIR infiltration and natural ventilation calculations (replaced by guide gu05), 1994, https://www.aivc.org/resource/tn-44-numerical-data-air-infiltration-and-natural-ventilation-calculations-replaced-guide. last Modified: 2023-01-20T09:54 + 01:00.

[49] Department of the Environment, Building Regulations 1991: Technical Guidance Document L – Conservation of Fuel and Energy, The Stationery Office, Dublin, 1991. Available at: https://assets.gov.ie/static/documents/technical-guidance-document-l-conservation-of-fuel-and-energy-1991-109-mb.pdf (Accessed 4 March 2026).

[50] Department of Housing, Local Government and Heritage, Building regulations 1997 technical guidance document l conservation of fuel and energy, The Stationery Office, Dublin, 1997. Available at: https://assets.gov.ie/static/documents/technical-guidance-document-l-conservation-of-fuel-and-energy-1997-128-mb-4259689d-6b8.pdf (Accessed 4 March 2026).

[51] Department of the Environment, Heritage and Local Government, Building Regulations 2002: Technical Guidance Document L – Conservation of Fuel and Energy – Dwellings, The Stationery Office, Dublin, 2002. Available at: https://assets.gov.ie/static/documents/technical-guidance-document-l-conservation-of-fuel-and-energy-dwellings-2002-6961-kb.pdf (Accessed 4 March 2026).

[52] Department of the Environment, Heritage and Local Government, Building Regulations 2007: Technical Guidance Document L – Conservation of Fuel and Energy – Dwellings , The Stationery Office, Dublin, 2007. Available at: https://assets.gov.ie/static/documents/technical-guidance-document-tgd-partl-conservation-of-fuel-and-energy-dwellings-2007-1.pdf (Accessed 4 March 2026).

[53] TABULA – Typology Approach for Building Stock Energy Assessment, Intelligent Energy Europe (IEE) project, European Commission, 2009–2012. Available at: https://episcope.eu/iee-project/tabula/ (Accessed 4 March 2026).

[54] EPISCOPE Irish Project Team, Monitoring the Energy Refurbishment Rates for the Housing Stock of the Northside of Dublin City, Technical Report, 2016.

[55] J. Kronvall, Testing of houses for air-leakage using a pressure method, 1978. https://www.aivc.org/resource/testing-houses-air-leakage-using-pressure-method. last Modified: 2015-08-12T17:19 + 02:00.

[56] A.K. PERSILY, Understanding Air Infiltration in Homes. Ph.D. thesis. Princeton University, 1982, https://www.proquest.com/openview/2ca33bddf96dfe25ac1a7d583eaf359d/1?pq-origsite = gscholar&cbl = 18750&diss = y.

[57] M.A. Makawi, I.M. Budaiwi, A.A. Abdou, Characterization of envelope AIR leakage behavior for centrally AIR-conditioned single-family detached houses, Buildings 13 (2023) 660, https://doi.org/10.3390/buildings13030660, https://www.mdpi.com/2075-5309/13/3/660. number: 3.

[58] S. Zheng, L. Zhao, Q. Li, Numerical simulation of the impact of different vegetation species on the outdoor thermal environment, Urban For. Urban Green. 18 (2016) 138–150, https://doi.org/10.1016/j.ufug.2016.05.008, https://www.sciencedirect.com/science/article/pii/S1618866716300413.